Pergamon

0301-9322(94)00072-7

Int. J. Multiphase Flow Vol. 21, No. 2, pp. 207–221, 1995
Copyright © 1995 Elsevier Science Ltd
Printed in Great Britain. All rights reserved
0301-9322/95 $9.50 + 0.00

GAS-PHASE SECONDARY FLOW IN HORIZONTAL, STRATIFIED AND ANNULAR TWO-PHASE FLOW

A. G. FLORES, K. E. CROWE and P. GRIFFITH
Department of Mechanical Engineering, MIT, Cambridge, MA 02139, U.S.A.

(Received 7 March 1994; in revised form 4 October 1994)

Abstract—Experiments were performed and semi-empirical correlations were developed to both prove the existence of gas-phase secondary flow and to predict annular to stratified transition limits for isothermal and heated horizontal annular two-phase flows in pipes. At the low vapor velocities, where this transition from stratified flow occurs and the entrainment/deposition mechanism is insignificant, secondary flow in the vapor core plays the principal role in the full development of the liquid annulus. Direct measurements of secondary flow are presented along with a simple model to correlate its behavior. The secondary flow model is used in conjunction with the fluid mechanics of the film to derive a boundary model for the onset of annular flow in this transition region. The resulting boundary agrees well with both the thermal and isothermal transition data.

Key Words: annular, dryout, horizontal, two-phase

1. INTRODUCTION

Horizontal, heated tubes find use in a wide variety of heat exchange components. These include once-through boilers and fluidized bed combusters (FBC). The use of horizontal tubes is driven by certain advantages inherent to this geometry. All else being equal, the two-phase pressure drop associated with horizontal tubes is lower than that for vertical up flow tubes. Also, horizontal flows display greater stability due to the absence of pressure drop–flow rate fluctuations inherent in down flow.

However, horizontal tubes suffer from an asymmetric liquid distribution which precedes dryout of the liquid film in the tube's upper half. Many researchers have used the term dryout interchangeably with burnout or critical heat flux (CHF), but in fact dryout is almost purely hydrodynamic in origin and can lead to unacceptably high wall temperatures even at a low heat flux.

It has been shown in the work of Ruder (1984), Ruder *et al.* (1987) and Crowe (1992) that dryout can be associated with three of the four major horizontal flow regimes and the mechanism governing its presence is different for each. Stratified flow is an inherently undesirable condition that can be avoided with a mass flux such that the Froude number, $Fr > 1$. Intermittent or slug flow can have intermittent occurrences of dryout which can lead to dangerous temperature oscillations of the tube wall. Both the results of Ruder (1984), Ruder *et al.* (1987) and Crowe (1992) showed that the intermittent dryout zone was a subset of the slug flow region and the liquid velocity needed to run in the intermittent regime without overheating was less than that required at the stratified limit. That is, the $Fr \geqslant 1$ limit is governing.

Dryout can also be associated with the annular flow regime as well. Essentially, this refers to the stratified–annular boundary where dryout in annular flow implies that the annulus is not complete. This boundary has been theoretically predicted by Taitel & Dukler (1976) and correlated with a large data set by Weisman *et al.* (1979). However, neither method addresses the specific mechanisms responsible for maintaining a complete liquid annulus. The air–water data of Flores (1992) are in good agreement with both models mentioned above and show that the annular flow transition is most strongly dependent on the gas-phase velocity. That is, there exists a superficial vapor velocity which is sufficient to bring the stratified liquid to the tube's top and the velocity is only weakly dependent on the liquid flux. The diabatic steam–water data of Crowe (1992) indicate a similar boundary and show that it is essentially independent of heat flux. In addition, it was found

(Crowe 1992) that increasing quality leads to another dryout where the liquid fraction in the tube is too small to allow for complete wetting of the tube wall. At these qualities, the vapor rate was quite high but it appears that insufficient entrainment/deposition is present to keep the pipe wet under the imposed heat loading.

The existence of horizontal, annular flow has been well documented but why it occurs is still unresolved. Mechanisms have been proposed but none can be decisively supported with data. The present paper attempts to answer some of the questions concerning the existence of horizontal annular flow. In particular it is shown that circumferential secondary flow in the vapor gas core exists. Through correlations and models it is also hypothesized to be the predominant cause of annular flow in the transition region between annular and stratified flows where the gas core flowrates are below or near the onset of entrainment. The approximate magnitude is measured and modeled for an analogous single phase flow and used to show its significance in keeping the tube top wet in an intermediate quality two phase flow.

2. MECHANISMS OF ANNULAR FLOW

Three mechanisms commonly accepted to play a role in producing/maintaining annular flow are entrainment/deposition, wave spreading and secondary flow in the gas core.

2.1. Entrainment/deposition

The onset of entrainment has been correlated over a wide database by Hewitt & Hall-Taylor (1970) as:

$$V_G = 1.5 \times 10^{-4} \sqrt{\frac{\rho_L}{\rho_G}} \frac{\sigma}{\mu_G}, \quad [1]$$

where V_G is the gas velocity, ρ_L is the density of the liquid, ρ_G is the density of the gas, σ is the surface tension between the gas and the liquid and μ_G is the viscosity of the gas. For air–water flow at atmospheric pressure, the critical velocity for the onset of entrainment is approximately 21 m/s. Higher velocities than those seen at the annular–stratified regime boundary are required for entrainment to become significant.

2.2. Wave spreading

In annular flow, the film's bottom layer is significantly thicker than that on the sides or tube top and is quite wavy due to imposed shear of the high speed vapor core. The speed of gravity waves in still water increases with depth. In a moving liquid, the fluid velocity also contributes to the overall wave speed. Both the depth and the fluid velocity are maximum at the pipe's bottom in horizontal annular flow. Therefore, wave fronts in this thick bottom layer do not display a uniform speed. As a result, wave crests oriented normal to the pipe axis initially, get tilted and have a component toward the wall (figure 1). With the force of the flowing gas on the wave, liquid can impact the pipe wall and be transferred up the wall in the same way that water moves up onto the beach as gravity waves approach the shore. This is known as *wave spreading*, and is generally accepted to aid in producing annular flow.

Recently Jayanti *et al.* (1990a) measured the time-dependent behavior of annular films in a horizontal pipe as a function of flow conditions and circumferential angle, θ, in degrees. With increasing vapor rate, the frequency content of the film thickness in the upper portion of the tube was similar to that of the bottom. It was concluded that, at high gas rates, there is circumferential spreading of liquid from the bottom, since the frequency characteristics appear to have come from the bottom.

However, it should be noted that at these high flow conditions, the thickness variation around the circumference of the tube is less than in the low flow cases, and it may be expected that the frequency content is dictated by both the film thickness and the gas velocity. However, there is no evidence that the liquid at the top is due to these waves. In addition, the gas flow rates being referred to correspond to $V_G = 70$ m/s which are well beyond the velocities of the present study.

Fukano & Ousaka (1989) predict the film thickness distribution in a 26 mm diameter pipe using a model built around the pumping action of disturbance waves. The authors also suggest the

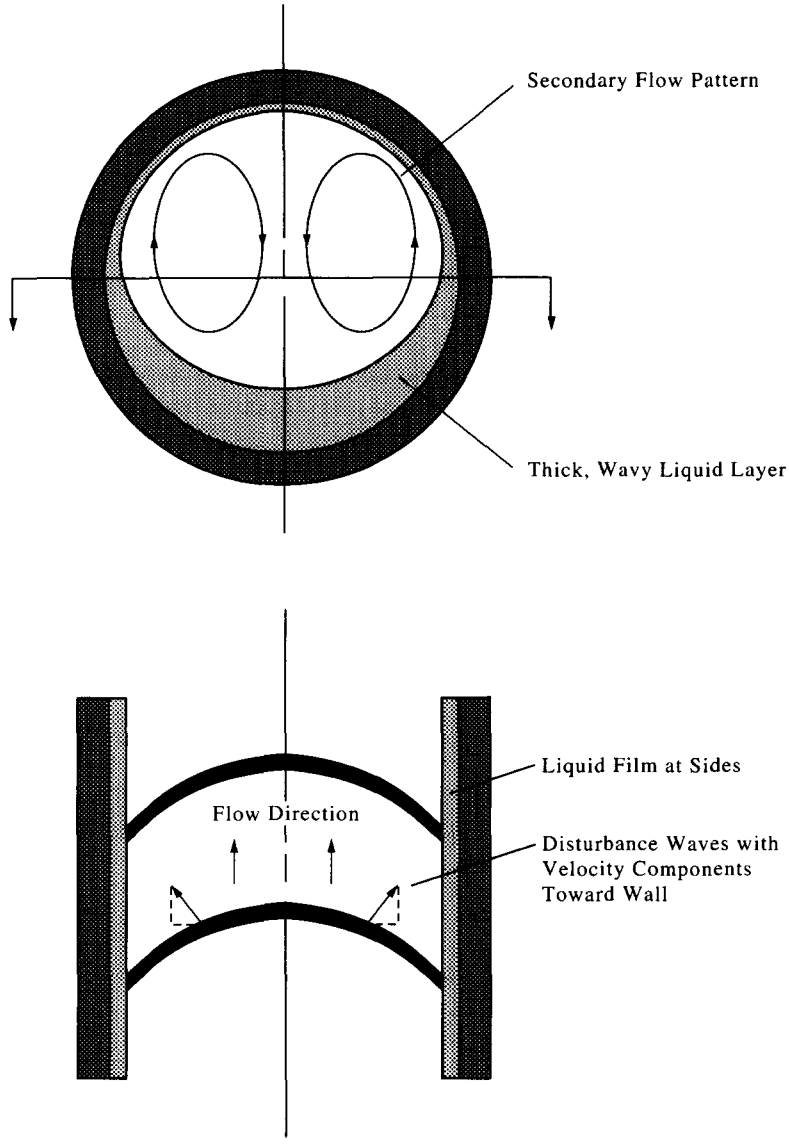

Figure 1. Sketch illustrating secondary flow and wave-spreading mechanisms.

existence of a top to bottom pressure gradient which will cause secondary flow but neglect the effect of the secondary flow on the film transport. Top to bottom pressure gradients have been measured (Flores 1992) in an asymmetrically roughened pipe which, as will be discussed, effectively mimics some important aspects of a horizontal stratified or asymmetric annular flow. Therefore, it would appear that disturbance waves are not essential to the development of a top to bottom pressure gradient. Nevertheless, the term in their analysis representing shear due to secondary flow is neglected. Although the agreement between their model and data is very good, the major objection to this work that the secondary flow mechanisms for bringing liquid to the top of the tube is excluded in favor of a new mechanism, that is not clearly explained. However, it is based on a circumferential pressure gradient, which is now known to exist in asymmetrically roughened pipe and is linked to secondary flow. In addition, it seems doubtful that small circumferential pressure gradients could transport liquid against gravity in the envelope of a disturbance wave, because the forces due to gravity should dominate the liquid flow for the wave thickness characteristic of this flow regime.

In flow visualization experiments, it was indeed observed that the disturbance wave envelope was quite thick. In no cases however, did any of the waves transport liquid beyond the mid plane of

the tube (Flores 1992). Based on this evaluation of the previous work, it would seem that wave spreading is a factor in producing annular flow. Though, at the low liquid flow rates near the dryout region of this investigation, there is no evidence that wave spreading transports liquid to the top of the tube.

2.3. Circumferential secondary flow

The role of secondary flow in the gas core in annular flow is rather controversial. Although no one has denied its presence as a possible driver, secondary flow has not been measured in the gas core of a horizontal annular flow. As a result, several researches have dismissed the mechanism as having negligible impact on this flow regime. Only in the present study has a direct observation of secondary flow in a horizontal stratified or annular flow been made.

The non-uniformity of film thickness in horizontal flow gives rise to circumferential dependence of film wave heights. Associated with the wavy film is an effective roughness and shape factor. In fact, Wallis (1969) correlates the average film thickness, δ_{av}, in annular flow to a skin friction coefficient, C_f, as:

$$C_f = 0.005\left(1 + 300\frac{\delta_{av}}{D}\right), \quad [2]$$

where D is the diameter of the pipe. Due to the asymmetry of the effective pipe roughness, the axial velocity profile is skewed so that the maximum gas velocity occurs at the bottom half of the tube (Jayanti *et al.* 1990b). It is believed that the secondary flow in the gas core occurs as the result of two things:

(a) Tilting and stretching of vortex rings, which is known as Prandtl's secondary flow of the first kind. This also occurs when a laminar flow goes around a bend.
(b) Anisotropy of the Reynold's stresses which is known as Prandtl's secondary flow of the second kind. This is strictly a turbulence phenomenon and has been measured in the corner regions of flow in non-circular cross sections (Hinze 1973).

Hinze (1973) has measured turbulent flow in rectangular ducts with asymmetric roughness and found that it satisfies a simplified turbulent kinetic energy relation. It essentially states that in regions where turbulent kinetic energy production exceeds viscous dissipation in a fully-developed flow, there must be an interchange of fluid from wall zones to the core. The secondary flow will always be toward the corner along the bisectrix in the case of non-circular ducts or along the normal toward a rough wall. Both of these are regions of high turbulence production. As will be seen in annular flow, the pipe bottom where the liquid carpet is thick and wavy is such a "rough" region and secondary flow is toward this carpet and back up the pipe walls as shown in figure 1. As depicted in this figure, the secondary flow takes the form of two counter-rotating axial vortices which can sweep liquid from the bottom (or sides) to the tube top.

Jayanti *et al.* (1990) studied the secondary flow mechanism in horizontal annular flow using a numerical computer simulation. Secondary flows were generated using wall roughness functions and empirical values. However, unlike the present study the researchers concluded the secondary values to be an order of magnitude less than those required to support the liquid film present in annular flow.

More concretely, Darling & McManus (1968) created an annular flow analog with an asymmetrically roughened pipe carrying a single phase air flow. Hot wire anemometer measurements revealed the flow pattern previously described. This work is significant for two reasons. First, it was found that the secondary velocity along the circumference scaled with the axial velocity, being about 4% of the average throughput velocity. Secondly, a connection between annular flow and asymmetry of wall roughness is made. As will be seen, this connection is a starting point for modeling secondary currents in horizontal annular flow.

In the course of studying the onset of annular flow, it was found that the vapor velocities are below the entrainment limit, or at least the entrained mass is very small. At these vapor velocities, it is expected that wave spreading (although believed to be a factor in maintaining annular flow) is not responsible for bringing liquid to the tube top. The results of Jayanti *et al.* (1990) support this as do the flow visualization studies of Flores (1992) where it was observed at the low gas

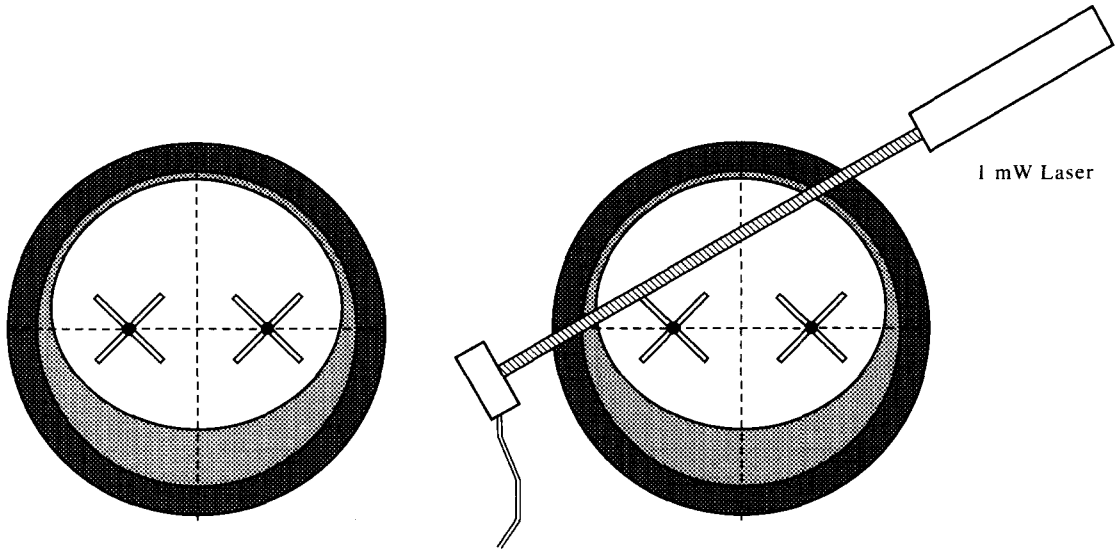

Figure 2 *(left)*. Vorticity meter placement in annular flow.
Figure 3 *(right)*. Secondary flow data acquisition set-up.

velocities in question (i.e. 21 m/s) that wave spreading did not progress past the mid plane of the tube (i.e. $\theta = 90°$).

3. EXPERIMENTAL INVESTIGATION

A series of experiments were performed to further explain the mechanism of secondary flow in the annular regime. The results of Darling & McManus (1968) suggest that the asymmetry of the pipe wall roughness gives rise to a secondary flow. Others have suggested the asymmetric shape formed by the liquid film alone causes secondary flows in the gas phase. In the present work it is desired to relate secondary flows to an effective wall roughness. With this relationship and a hydrodynamic model or the liquid film, the dryout boundary can then be predicted.

3.1. Dryout experiments

In order to validate the predictions for dryout discussed later, dryout boundaries were mapped out in both atmospheric pressure air–water and steam–water systems. The air–water system consists of 5.08 cm tubing 3 m long (Flores 1992) while the steam–water system consists of 5.7 cm tubing 4 m long and supported variable heat flux loading (Crowe 1992). These data also support the fully developed state of the annular flow, for the dryout data agree well with that of other researchers using much greater length over diameter, L/d, values (figures 9 and 10).

3.2. Evidence of secondary flow—air–water experiments

To visibly capture the existence of secondary flows in the gas core, the air–water test rig was used. The secondary current was measured using a twin axial vorticity meter. The 1.9 cm plastic paddle wheels were held into the wire frame with low friction, Teflon bearings. The entire frame was inserted into the pipe end and positioned as shown in figure 2.

When air alone was passed through the pipe, the two rotors remained stationary. By simply adding a small water flow (which traveled along the tube bottom), both rotors would commence turning in constant counter rotations in the directions described in figure 1. An increase in either the air rate or the water rate increased the rotation rate from the stratified-wavy regime into the annular flow regime. Once the fluid flow was turned off, the rotors would stop turning and remain motionless. This phenomenon during annular flow was captured on video and displayed angular velocities on the order of 5 rev/s (Flores 1992). It should be noted that the rotation directionss was always consistent with the previously described directions. This is the first known direct verification of the existence of circumferential secondary flow in the annular regime.

3.3. Asymmetric roughness experiments

A 3 m long clear PVC pipe was severed along the mid-plane and the lower half was artificially roughened by gluing different roughnesses to the inside surface while the upper half remained smooth. The values of roughness heights varied between 0.00031 and 0.002 m with each test having a distinct value. The two halves were reassembled and connected to the air supply.

The air velocity was measured using a Pitot tube and the rotation rate of the vorticity meter was determined using the laser system shown in figure 3. The rotation rate was found from counting the pulsed output of intensity vs time measured at the photodetector. The rotors turned in the direction consistent with that of annular flow and the results of Darling & McManus (1968). The rotation rates were measured as a function of axial flow rates for four different roughnesses.

The rotors were placed in the tube's cross section in the same manner as those in figure 2. It was believed the average value of the secondary flow was obtained in this position. This was verified by placing the meter in several other cross-sectional locations within the tube at which the angular velocities were measured and displayed very little variance (Flores 1992).

The results of the measurements for the entire set of tests are shown in figure 4 along with this empirical correlation relating the angular rotation, ω, to axial velocity and roughness height, ε:

$$\omega = 1.07 V_G \log\left(\frac{1000\varepsilon}{0.03}\right). \quad [3]$$

The mean secondary velocity values, V_s, can be inferred from the angular rotation rates by multiplying by the radius of the rotor. It can be easily seen that the secondary flows are on the order of a few percent of the axial flows consistent with the experiments of Darling & McManus (1968).

3.4. Shape factor experiment

At the annular flow/stratified flow dryout boundary, the liquid at the tube's bottom forms an asymmetric shape through which the gas flows. Many have speculated that this asymmetric path may induce secondary flows in the gas phase. An experiment was performed that displayed shape factor-induced secondary flows on the same magnitude as those in the roughness experiments.

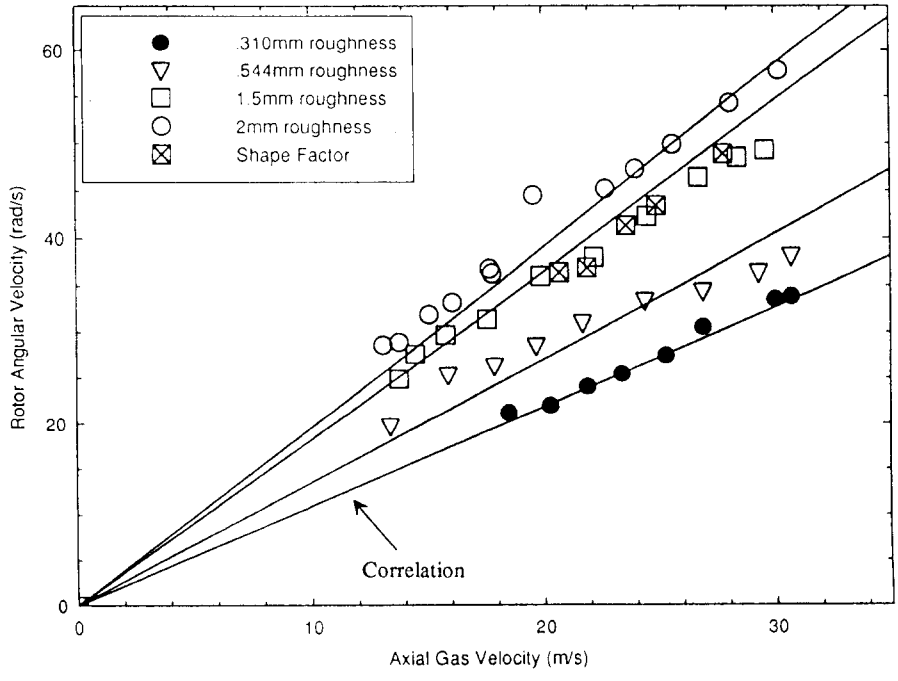

Figure 4. Secondary flow data for shape factors and various roughness heights.

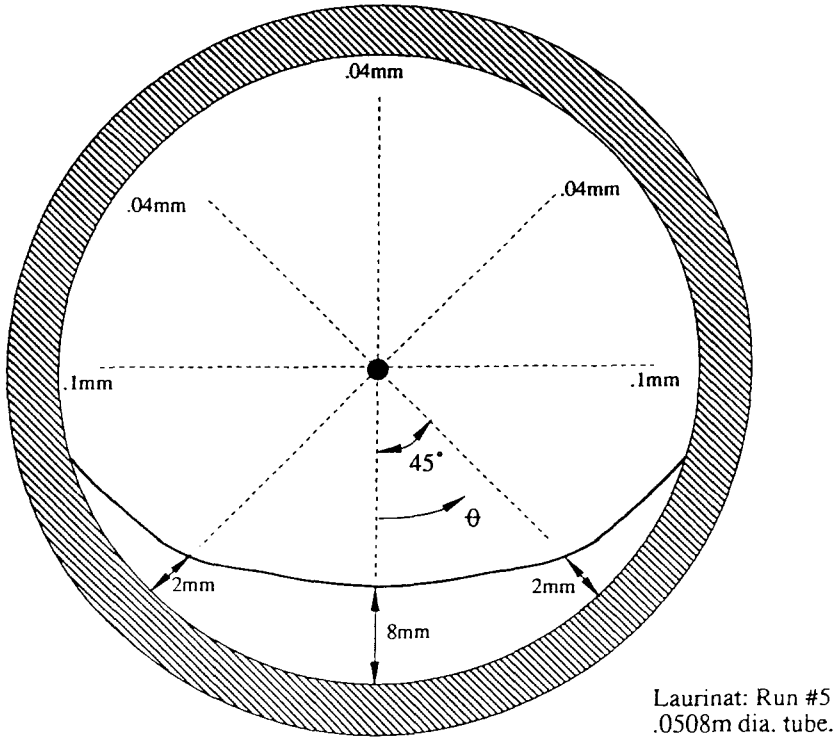

Figure 5. Laurinat's (1982) air–water film thickness profile for annular flow in a 0.0508 m diameter tube near dryout.

Annular film thickness dimensions near dryout in 0.0508 m diameter tubes as measured by Laurinat (1990) were mimicked with molds (figure 5). The plaster of Paris molds were inserted 20 diameters into the tube. Gas was forced through the tube over the asymmetric shape, and the rotation of the vortex meters was measured as a function of axial gas velocity in the same manner as the roughness experiments. The results are plotted along with those of the roughness experiments (figure 4). However, it should be noted that unlike the roughness tests, the secondary flows diminished to negligible values when the mold extended to 60 L/Ds into the tube. Due to the transient patterns produced by waves, it was concluded that the secondary flows caused by shape may be lumped into an effective roughness characterized by the liquid film's thickness, δ and void fraction, $1-\epsilon$.

3.5. Differential pressure measurements

To gain further evidence and understanding of the secondary flow, experiments were performed to see if there is an associated circumferential pressure gradient in these asymmetric flows. It was hypothesized that the flow must actually be driven by a pressure difference but neither magnitude nor the gradient was known.

The experiments were carried out in the half roughened pipe apparatus described earlier. The details of the experiment can be found in Flores (1992). Basically, the differential pressure between the bottom and top of the tube was measured using 0.001 m diameter pressure taps at a location far downstream of the pipe inlet. The square edged taps were connected to a high precision manometer. The differential pressure between the bottom and the top of the tube's cross-section, defined as $p_b - p_t$, was measured for the various air flow rates and roughnesses employed in the previous experiments.

Several tap geometries and arrangements were employed (Flores 1992) to diminish the local effects of the roughness elements and the tap edge. The cumulative data, although scattered, showed in all cases that the pressure difference is positive, i.e. the pressure at the center of the rough

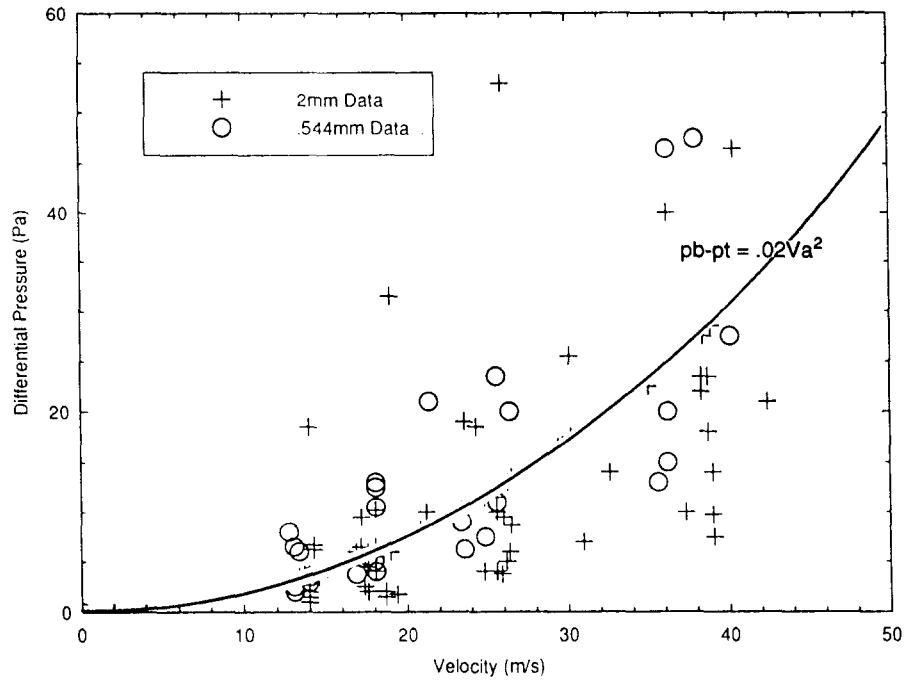

Figure 6. Cumulative differential pressure data and correlation.

(bottom) wall at a given axial location is always higher than the pressure at the center of the smooth (top) wall.

To an order of magnitude, the pressure difference can be approximated as:

$$p_b - p_t \approx \frac{1}{2}\rho_G V_G V_s. \quad [4]$$

Since the secondary velocity was found to be proportional to the axial component, for a fixed roughness, it is clear that the pressure difference goes like the square of the flow rate. Equation [4] is plotted along with the results of the differential pressure measurements in figure 6 showing the same order of magnitude behavior. The curve plotted in figure 6 is derived assuming a secondary velocity equal to 4% of the gas velocity and a gas density of 1 kg/m^3.

4. MODELING AND RESULTS

At gas velocities below or near the onset of entrainment, secondary flows seem the most likely mechanism responsible for transporting liquid from the mid-plane of the tube's wall to its top at the stratified to annular flow regime boundary. Wave spreading as the visual studies display (Flores 1992), transport liquid from the bottom of the tube up the tube's walls to approximately the mid-plane in a wide range of fluid flow rates. At higher gas flow rates, it is believed the entrainment/deposition mechanism is responsible for further supporting and distributing the liquid film. Thus, if one were to fully determine the film/gas behavior in the annular flow regime all the aforementioned mechanisms must be included in the analysis. However, it appears that near dryout, if the magnitude of the secondary flow is known and the liquid film is properly modeled, dryout limits could be suggested.

4.1. Secondary flow

Secondary flows in the gas core result in a shear imposed in the vertical direction on the liquid film. This shear in the secondary flow direction at the tube's walls, τ_s, can be related to the shear of the gas on the liquid in the axial direction, τ_a, in the same manner as pressure differentials

described earlier (Flores 1992). The resulting equation is:

$$\tau_s \approx \tau_a \frac{V_s}{V_G}. \quad [5]$$

Wallis gives a friction factor for axial interfacial shear in annular flow in [2] which results in an axial shear of:

$$\tau_a \approx 0.0025\left(1 + 300\frac{\delta_{av}}{D}\right)\rho_G V_G^2. \quad [6]$$

Since the liquid velocities and flow rates are very small in the dryout region being explored, the actual and superficial gas velocities are assumed to be approximately equal. Substituting [6] into [5] gives:

$$\tau_s \approx 0.0025\left(1 + 300\frac{\delta_{av}}{D}\right)\rho_G V_G V_s. \quad [7]$$

The secondary velocity correlation developed in [3] gives angular speed of the rotors versus axial velocity of the gas and roughness height. Assuming approximate solid body rotation in the vorticies [3] can be transformed to velocities. The conversion is performed by multiplying the angular velocity by 1/4 the diameter of the tube. The gas density is also tied into the correlation using the parameter relationship of a pressure drop formula. Thus, [3] becomes:

$$V_s \approx 0.268 D\rho_G^{0.5} \log\left(\frac{1000\varepsilon}{0.03}\right). \quad [8]$$

In annular flow with thin films, Wallis equates roughness to approximately four times the circumferential averaged film thickness changing [8] to:

$$V_s \approx 0.268 D\rho_G^{0.5} V_G \log\left(1.33 \times 10^5 D\frac{\delta_{av}}{D}\right). \quad [9]$$

From the geometry of an annular film:

$$4\frac{\delta_{av}}{D} \approx (1 - \epsilon). \quad [10]$$

Substituting [9] and [10] into [7] gives:

$$\tau_s \approx 6.7 \times 10^{-4} D\rho_G^{1.5} V_G^2 [1 + 75(1 - \epsilon)]\log[3.33 \times 10^4 D(1 - \epsilon)]. \quad [11]$$

With [11] secondary shear values can be derived for any set of two-phase flow parameters near the annular flow regime using the Martinelli parameter's relationship to void fraction. The Martinelli parameter, X, is defined as the square root of the fluid pressure drop divided by the gas pressure drop if each phase were flowing alone in the tube. In annular flow the majority of the flows are turbulent–turbulent and the Martinelli parameter simplifies to (Wallis 1969):

$$X^2 \approx \frac{\rho_L V_L^2}{\rho_G V_G^2}, \quad [12]$$

where, V_L, is the velocity of the fluid phase. Using [12] secondary shears can be found for any set of flow parameters by looking at figure 7 and matching the proper X value with the given void fraction or vice versa. An approximate equation for figure 7 is given by (Wallis 1969):

$$X = \frac{[(1 - \epsilon)^2[1 + 75(1 - \epsilon)]]^{1/2}}{\epsilon^{5/4}}. \quad [13]$$

Thus, secondary velocities and their resulting shears can be determined in close form with the superficial gas and liquid velocities.

4.2. Liquid film

When modeling the liquid film several facts must be considered. First, the secondary shear pattern and tube geometry must be modeled. Second, the type of flow must be determined, i.e.

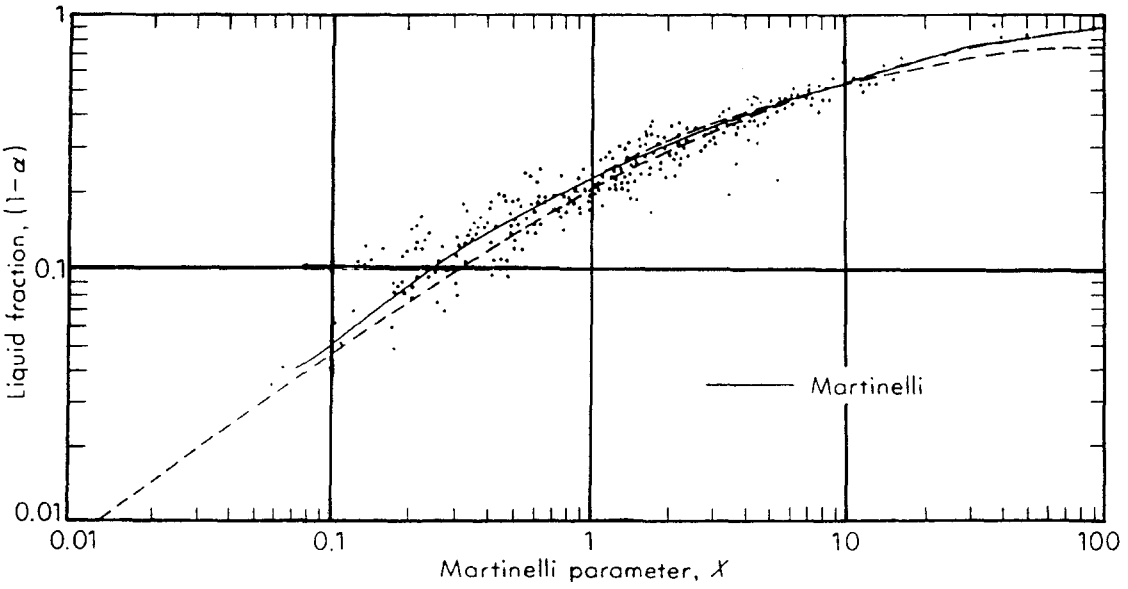

Figure 7. Liquid void fraction vs Martinelli parameter.

laminar or turbulent. Lastly, certain two-phase phenomena must be applied to the model such as flooding and wall shear stress limits. Near dryout, the liquid film's thickness is assumed to be approximately equal throughout the top half of the tube. The film thickness data from Laurinat (1990) near the dryout limit verifies this assumption to within a few percent. The data from Darling & McManus (1969) also gives that the strength of the secondary flow velocities and induced shears, vary with the sine of the angular position at which the bottom of the tube corresponds to zero degrees. In other words, halfway up the tube, or at 90° the secondary velocity is at its greatest value. From a force balance on the liquid film, it is obvious that the force required to hold the film up the walls of the tube also varies with the sine of angular position. Thus, near the dryout limit, the decay of secondary shear and the required shear to hold up the liquid film are assumed to cancel resulting in approximately the same film thickness throughout the upper half of the tube. With this in mind, the film thickness model simplifies to that of the liquid film at 90° (figure 8).

Since both flows are considered turbulent (Lockhart & Martinelli 1949), the liquid film must be described with turbulent characteristics such as eddy diffusivities and viscous sub layer. The turbulent friction velocity, u_*, is defined by:

$$u_* = \sqrt{\frac{\tau_a}{\rho_L}}. \qquad [14]$$

The shears used to determine the friction velocity in the film should be taken from the axial flow in the tube since they are much greater than the shears associated with the secondary flows. Thus, the axial film determines the amount and magnitude of turbulence. In a given annular flow, the axial film flow can be assumed fully-developed with little or no significant pressure gradient. Therefore, in the axial direction the wall shear stress is equal to the interfacial shear stress on the film given by [6]. In turbulent flows near stationary boundaries, the viscous sub layer is prevalent until y^* is approximately equal to 5. The turbulent length scale, y^*, is given by (Tennekes 1990):

$$y^* = \frac{yu_*}{\nu_L}, \qquad [15]$$

where y is the height and ν_L is the kinematic viscosity of the liquid.

Laurinat (1990) gives a film thickness in the upper half of the tube on the order of 0.00004 m near dryout. In an air–water flow with a gas velocity of 30 m/s and a film thickness of approximately 0.00004 m the viscous sub layer would go out to 0.00009 m. Thus, the *entire film* near the dryout limit is approximated to be within the viscous sub layer and behaves in a

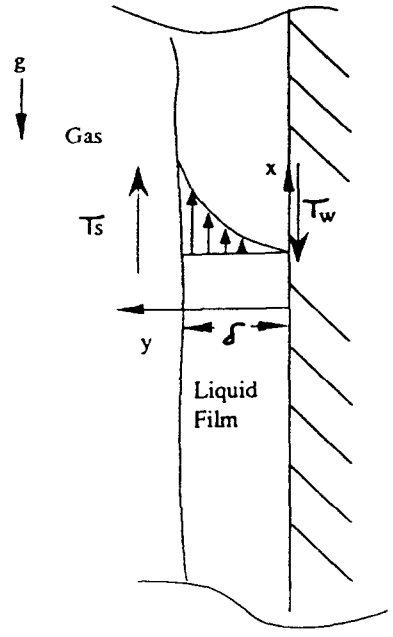

Figure 8. Uniform film thickness and secondary shear relationship.

statistically laminar fashion. Consequently, the film near the dryout limit in the upper half of the tube is approximated as being within the viscous sub layer.

When dealing with gravity, g, driven films as in our model, certain empirical facts must be taken into account. Using the analogy of film flooding in gas–liquid flows in vertical tubes, the film's velocity profile must be all traveling in one direction for a stable film to exist (Hewitt 1963). In other words, for any fluid to travel up to the tube's walls, the shear at the film's interface must be great enough to push the entire film upwards against gravity. At the limit of a stable vertical film flowing upwards, the shear at the wall equals zero. The dryout model will use this limit to relate shears and film thicknesses.

The previous assumptions define all variables required to model the liquid film–secondary flow relationship. Using figure 8 a force balance is performed on the film assuming the shear at the wall is equal to zero giving:

$$\tau_s = (\rho_L - \rho_G)g\delta, \qquad [16]$$

where δ is the film thickness.

With the a no slip boundary condition and zero wall shear stress, the Navier–Stokes equations reduce to simple terms and result in:

$$\bar{u}(y) = \frac{(\rho_L - \rho_G)gy^2}{2\mu_L} \qquad [17]$$

and

$$Q' = \frac{(\rho_L - \rho_G)g\delta^3}{6\mu_L} \qquad [18]$$

where $\bar{u}(y)$ is the mean velocity distribution and Q' is the vertical film flux up the tube's walls.

The model describing the film displays a net mass flux up the sides of the tube near the dryout boundary in adiabatic systems. This net mass flux in the film could account for a certain robustness of the dryout limit with respect to a range of heat fluxes in two-phase flows involving heat transfer. In other words, there may exist in the film an abundance of net mass flux up the walls of the tube to account for the amount of liquid being evaporated into vapor. Since the flow is assumed to be fully developed, the net mass flux in the film traveling up the tube's walls must either collect at

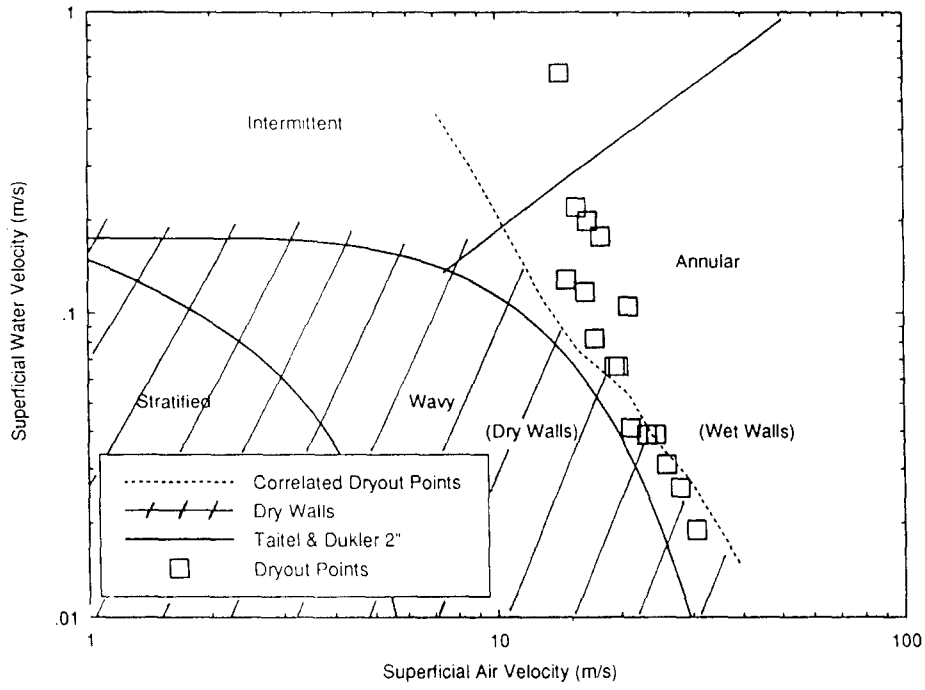

Figure 9. Adiabatic air–water experimental and correlated dryout boundaries.

the tube's top and drop down in a transient manner, be entrained in the gas core, or evaporate due to the boiling and heat transfer in the upper half of the tube.

4.3. Dryout limit

With the previously described model and secondary shear correlation, the air–water dryout data from section 3 can be used to find a critical film thickness associated with dryout in adiabatic systems. Superficial gas velocities and fluid velocities equal to 30 and 0.018 m/s respectively, are arbitrarily chosen from the dryout points mapped in section 3. Using [12] gives a Martinelli parameter value of 0.019 which corresponds to a liquid fraction of 0.015. Substituting into [10] and then [16] results in critical film thickness of 0.00001 m. It is interesting to note that this value is on the order of the film thickness measured by Laurinat (1990) just preceding dryout in the same flow situation. It is believed this critical film thickness prevails due to certain hydrodynamic factors such as surface tension, viscosity and density. Thus, the film thickness value of 0.00001 m is taken as a limit for dryout in adiabatic two-phase flows in 5.08 cm tubes. The corresponding superficial gas and liquid velocities that result in this value are determined through [16] and [10]. This boundary is plotted along with the actual air–water dryout points of section 3 (figure 9). The dryout boundaries are almost identical and give validity to the model's behavior.

The model can also be used to find dryout boundaries in similar systems where heat transfer is present. At dryout in systems with heat transfer, it is assumed that the liquid film's mass flux up the sides of the tube's walls given by [18] is evaporated into vapor to account for the heat flux in the upper half of the tube. The relationship between heat flux, q', and the critical Q' is given by:

$$Q' = \frac{q'\pi D}{4\rho_L h_{LG}}, \qquad [19]$$

where h_{LG} represents the latent heat.

The critical film thickness and secondary shears then become:

$$\delta = \left(\frac{3q'\pi D\mu_L}{2\rho_L h_{LG}(\rho_L - \rho_G)g} \right)^{1/3} \qquad [20]$$

and

$$\tau_s = (\rho_L - \rho_G)^{2/3}\left(\frac{3q'\pi D\mu_L}{2\rho_L h_{LG} g}\right)^{1/3}. \quad [21]$$

Using the critical secondary shear from [21], the dryout boundary's superficial gas and fluid velocities can be found.

The dryout data of Crowe (1992) of steam–water flows at atmospheric pressure in 0.057 m diameter tubes display little variation in the dryout boundary due to differences in heat flux. Since mass flux or Q' varies with the cube of secondary shear and film thickness, this behavior also tends to verify the model's behavior. Thus, a change in the required film mass flux due to different heat fluxes would result in a very small critical film thickness variation, and the resulting dryout boundaries would only slightly differ from one another. Crowe's experimental heat flux values fell in the range of 30–150 kW/m^2. Although this independence of heat flux behavior will change at extremely high heat fluxes, most designs of boilers, and heat exchangers also fall in the 30–150 kW/m^2 heat flux range. Solving for the required secondary shears and dryout boundaries, the model and experimental data can be compared (figure 10). The actual and correlated boundaries again lie very close to one another proving the validity of the model's behavior.

4.4. Specific modeling instructions

The dryout boundary can be found using the following modeling scheme:

Step 1: Determine the critical film thickness:
- (a) In a system with no heat transfer, use the critical film thickness of 0.00001 m.
- (b) If the system has heat flux find the critical film thickness with [20] and the systems properties. Take 0.00001 m as the critical film thickness if the value from [20] is smaller than 0.00001 m.

Step 2: With the critical film thicknesses found in step 1 determine a critical shear with [16].

Step 3: Knowing the critical shear from step 2, solve for gas velocity versus void fraction using [11].

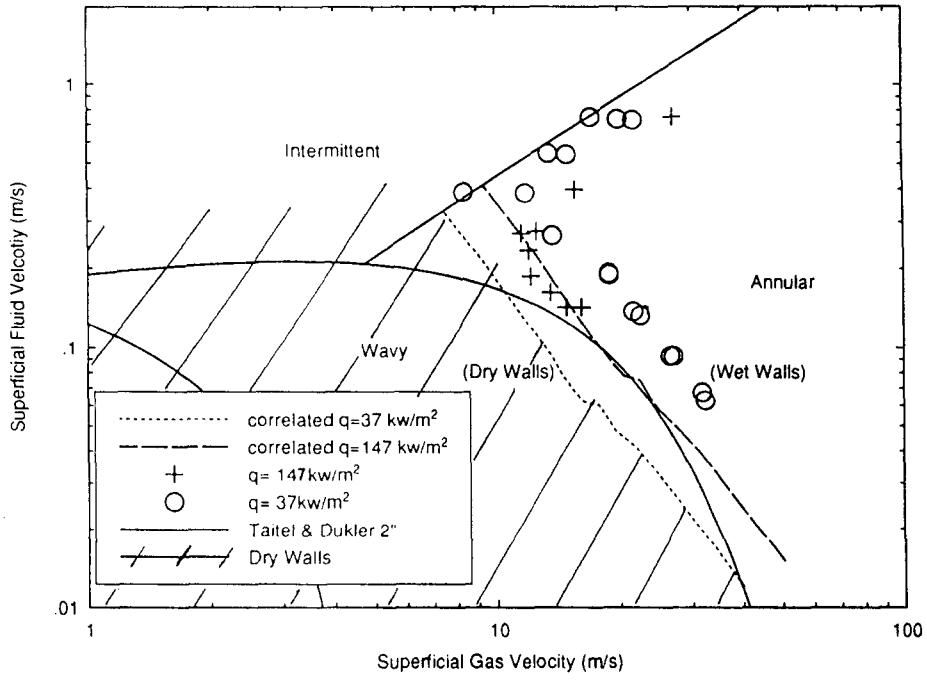

Figure 10. Steam–water experimental and correlated dryout points at 1 atm for various heat fluxes.

Step 4: Take a void fraction value from step 3 and find the corresponding Martinelli parameter with figure 7 or [13]. With the gas velocity corresponding to the void fraction from step 3 and the Martinelli parameter from step 4, solve [12] for fluid velocity. The superficial fluid and gas velocities developed through this process define a dryout point. Continue this process for a wide range of void fraction–gas velocity combinations from step 3 to define the entire boundary.

5. DISCUSSION

In the present experiments, the range of gas velocities where the stratified–annular transition takes place would imply that neither the wave-spreading nor the entrainment/deposition mechanism can significantly control the onset of annular flow. The first order model and roughness correlation would seem to support the ability of the secondary flow mechanism to transport liquid to the top of the tube.

Although the models and correlations presented here should not be strictly used to establish dryout criteria, their overall behavior and symbiotic relationships should contribute valuable insights into the controlling mechanisms of annular flow and dryout. The roughness correlation produces believable results when compared to the actual secondary flows measured in annular flow while being based on logical conclusions and the well-known correlations of Wallis (1969). The critical film thickness for adiabatic flows was chosen from empirical data and perhaps could be better explained with some sort of dimensional analysis relating hydrodynamic properties. Notwithstanding these points, the model's behavior and results agree surprisingly well with the experimental data.

Putting the model and correlations aside, the most important achievement of this work is the positive proof of secondary flows in horizontal annular flow. The phenomenon was captured on video tape and displays flows in the directions hypothesized by earlier researchers. The existence of secondary flows can no longer be discounted in annular flow.

6. CONCLUSION

The experimental and analytical investigations produced new insights regarding the cause of the annular–stratified flow regime dryout boundary and the liquid film transport phenomenon. Several potential mechanisms related to film transport in annular flow were investigated to find the most dominant near dryout. The major results of the study are as follows:

—*Secondary flows do exist in the annular flow regime in horizontal tubes.*
—The secondary flows are a result of both the circumferential roughness variation of the liquid film, as witnessed by the gas flow, and the asymmetric shape caused by the same film thickness variation. Any roughness variation, step or continuous, will cause this secondary flow.
—At low gas velocity the major factor which transports liquid into the upper half of the tube causing the transition from the stratified to annular flow is the circumferential secondary flow in the gas core. At higher gas velocities, the deposition of entrained liquid is a more significant factor in transporting liquid to the top of the tube.
—A model is presented using a first order analysis and established correlations which captures the proper dryout behavior and magnitude in tubes of approximately 0.0508 m diameters.

REFERENCES

CROWE, K. E. 1992 Flow regimes and dryout limit in heated horizontal pipes. Ph.D thesis, MIT, unpublished.

DARLING, R. S. & MCMANUS, H. N. Jr 1968 Flow patterns in circular ducts with circumferential variation of roughness: a two-phase analog. *Developments in Mechanics: Proceedings of the 11th Midwestern Mechanics Conference*, Vol. 5, pp. 153–170.

FLORES, A. G. 1992 Dryout limits in horizontal annular flow. S.M. thesis, MIT, unpublished.

FUKANO, T. & OUSAKA, A. 1989 Prediction of the circumferential distribution of film thickness in horizontal and near-horizontal gas–liquid annular flows. *Int. J. Multiphase Flow* **15,** 403–419.

HEWITT, G. F. & TAYLOR, N. S. 1970 *Annular Two-phase Flow*. Pergamon Press, Oxford.

HEWITT, G. F. & WALLIS, G. B. 1963 Flooding and associated phenomena in falling film flow in a tube. In *Proceedings of the ASME Multi-phase Symposium*, p. 62.

HINZE, J. O. 1973 Experimental investigation on secondary currents in the turbulent flow a straight conduit. *Appl. Sci. Res.* **28,** 453–465.

JAYANTI, S., HEWITT, G. F. & WHITE, S. P. 1990 Time-dependent behaviour of the liquid film in horizontal annular flow. *Int. J. Multiphase Flow* **16,** 1097–1116.

JAYANTI, S., WILKES, N. S., CLARKE, D. S. & HEWITT, G. F. 1990 The prediction of turbulent flows over roughened surfaces and its application to interpretation of mechanisms of horizontal annular flow. *Proc. R. Soc. Lond. A* **431,** 71–83.

LAURINAT, J. E. 1982 Studies of the effects of pipe size on horizontal annular two-phase flows. Ph.D. thesis, University of Illinois at Urband-Champaign, unpublished.

LOCKHART, R. W. & MARTINELLI, R. C. 1949 Proposed correlation of data for isothermal two-phase, two-component flow in pipes. *Chem. Engng Prog.* **45,** 39.

RUDER, Z. 1984 The influence of two-phase flow regimes on circumferential temperature distribution in horizontal, steam generating tubes. Ph.D. thesis, Department of Mechanical Engineering, Ben Gurion University, Israel, unpublished.

RUDER, Z., BAR-COHEN, A. & GRIFFITH, P. 1987 Major parametric effects on isothermality in horizontal steam generating tubes at low and moderate qualities. *Int. J. Heat Fluid Flow* **8,** 218–227.

TAITEL, Y. & DUKLER, A. 1976 A model for predicting flow regime transitions in horizontal and near horizontal gas–liquid flow. *AlChE Jl* **22,** 47–55.

TENNEKES, H. & LUMLEY, J. L. 1972 *A First Course in Turbulence*. MIT Press, Cambridge, MA.

WALLIS, G. B. 1969 *One-dimensional Two-phase Flow*. McGraw–Hill, New York.

WEISMAN, J., DUNCAN, D., GIBSON, J. & CRAWFORD, T. 1979 Effects of fluid properties and pipe diameter on two-phase flow patterns in horizontal lines. *Int. J. Multiphase Flow* **5,** 437–462.